ADVANCED MATERIALS INTERFACES
Open Access
www.advmatinterfaces.de

Pulse Duration Dependent Formation of Laser-Induced Periodic Surface Structures in Atomic Layer Deposited MoS_2

*Malte J. M. J. Becher, Jonas B. Ullrich, Julia Jagosz, Aleksander Kostka, Claudia Bock, Andreas Ostendorf, and Evgeny L. Gurevich**

In this paper, the formation of laser-induced periodic surface structures (LIPSS) on atomic-layer deposited MoS_2 layers are studied experimentally. The process parameters (laser fluence and the pulse overlap) corresponding to formation of low- and high-spatial frequency LIPSS as well as ablation and modification of the layers are identified for different pulse durations in the range from 0.2 to 10 ps. The role of the temperature accumulation is evaluated by changing the repetition rate from 0.2 to 2 MHz. The negative accumulation effect, i.e., the ablation of the layers becomes more difficult at higher laser pulse overlaps, is also observed. A simple model explaining the transition between different types of the LIPSS and the decrease of the ablation efficiency with the pulse overlap is suggested.

1. Introduction

The laser-induced periodic surface structures (LIPSS) or ripples are formed by laser radiation on surfaces of different materials like e.g., metals, semiconductors and dielectrics.[1,2] The period of such patterns is either approximately one order of magnitude smaller than the laser wavelength (in this case they are referred to as HSFL or high-spatial frequency LIPSS) or comparable to the laser wavelength (referred to as LSFL or low-spatial frequency LIPSS). The latter can be controlled either by the laser wavelength or by changing the processing environment, the orientation - by the incident light polarization.[3–5] Although the formation mechanisms of the periodic structures are not completely understood, the main players are agreed to be either interference, or hydrodynamics, or an interplay of these two processes.[6,7] The LSFL can be assigned to the interference between the incident and the surface-scattered waves[8] but the formation of HSFL, which period is much smaller than the laser wavelength is less understood.

Recently LIPSS in thin layers attracted much attention: periodic highly-ordered regular ripples were reported in different metal films like Cr, Hf, W, and Ni.[9–12] 2D materials represent a new class in the ultra-thin film region and are famous for their properties and possible applications in different fields like e.g., photonics and optoelectronics.[13,14] To implement these materials in electric devices, the main modification tasks are crystallization[15] and patterning. Direct laser writing is a powerful patterning tool of thin layers, but the minimal feature size is limited by the optical resolution,[16] which can be overcome but at the cost of throughput and price. However self-organization processes open an attractive alternative way of nanopatterning, especially if the geometry can be controlled. The self-organized periodic surface structures have been reported in multi-layer graphene,[17] reduced graphene oxide[18] and MoS_2.[19–21] The groups around Zuo et al., and Salimon et al., showed, that the structuring of the MoS_2 films can increase the optoelectronic properties of unstructured films and enable the applications as electronic devices based on MoS_2 such as logic circuits, chemical sensors, and p-n diodes.[19,20] High-spatial frequency LIPSS in such 2D materials can be an easy way of rapid large-area generation of nano-wires, however the reproducible patterning requires a deeper understanding of the pattern formation processes.

In our previous, publication we demonstrated the LIPSS formation in MoS_2 layers with fs laser pulses and studied the range of laser processing parameters (scanning velocity and average laser power) corresponding to the formation of these structures.[21] In this paper, we extend the previous experiments

M. J. M. J. Becher, J. B. Ullrich, A. Ostendorf
Ruhr-Universität Bochum
Applied Laser Technologies
Universitätsstraße 150, 44801 Bochum, Germany

J. Jagosz, C. Bock
Ruhr-Universität Bochum
Microsystems Technology
Universitätsstraße 150, 44801 Bochum, Germany

A. Kostka
Ruhr-Universität Bochum
Center for Interface Dominated Materials
Universitätsstraße 150, 44801 Bochum, Germany

E. L. Gurevich
University of Applied Sciences Münster
Laser Center (LFM)
Stegerwaldstraße 39, 48565 Steinfurt, Germany
E-mail: gurevich@fh-muenster.de

E. L. Gurevich
Center for Lasers and Optics
Anhui University
Hefei 230088, China

The ORCID identification number(s) for the author(s) of this article can be found under https://doi.org/10.1002/admi.202400478

DOI: 10.1002/admi.202400478

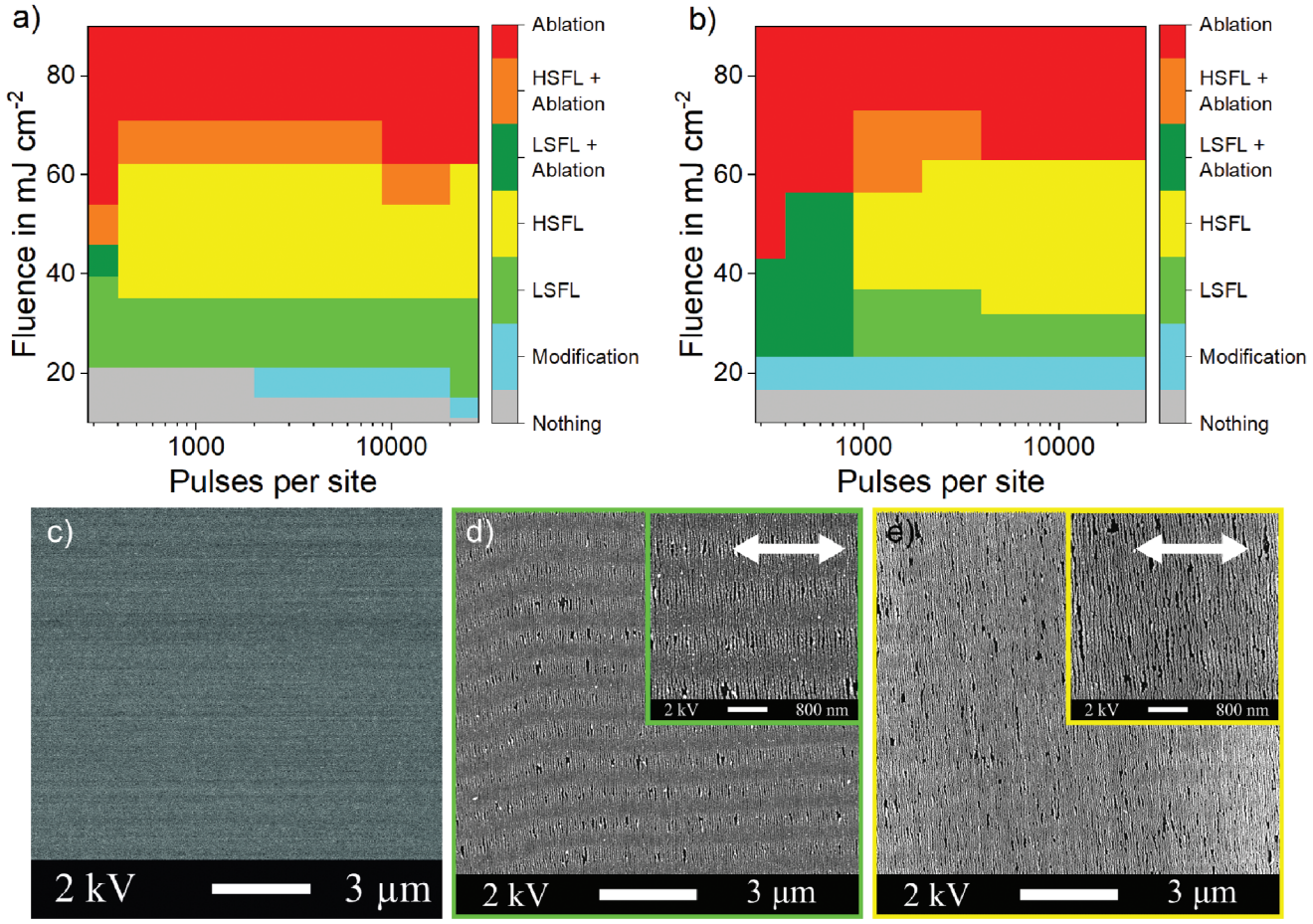

Figure 1. Fluence and pulses per site depended on LIPSS appearance in a 40 nm thick MoS_2 film on SiO_2/Si substrate, with a repetition rate a) f_{rep} = 200 kHz and b) f_{rep} = 2 MHz and a pulse duration t_p = 200 fs. SEM images of the c) pristine PE-ALD deposited surface d) LSFL formation (F = 26.2 mJ cm^{-2} and O = 45000 pls per site) and (e) HSFL formation (F = 45.0 mJ cm^{-2} and O = 45000 pls per site) at f_{rep} = 200 kHz and t_p = 200 fs.

varying the laser pulse duration and provide a model explaining the transitions between different experimentally-observed patterns. Moreover, we observe the "negative accumulation effect" in MoS_2, i.e., an increase of the ablation threshold with growing number of the laser pulses and present a model explaining this effect.

2. Experimental Set-Up

2.1. Atomic Layer Deposition of MoS_2

A plasma-enhanced atomic layer deposition (PE-ALD) process[22,23] was used to deposit a MoS_2 film on a silicon-dioxide (d = 200 nm)/silicon substrate. The substrate temperature was $T_{sub} \approx 230\,°C$ due to limited thermal contact between the substrate and the table (T = 300 °C). The MoS_2 film was deposited using a SENTECH Instruments GmbH SI ALD reactor equipped with a remote capacitively coupled plasma source (f = 13.56 MHz). The precursor, Bis(t-butylimido)bis(dimethylamino)molybdenum (Strem, 98 %) was heated in a stainless-steel canister to T = 50 °C. A 100 sccm (standard cubic centimeters per minute) nitrogen bubbling flow rate was applied to facilitate precursor delivery into the reactor. A plasma mixture of 5 sccm hydrogen sulfide (99.5 %) and 45 sccm argon was used as the co-reactants. The plasma was operated at a power of 200 W at a pressure of 10 Pa. For a detailed description of the process and the characterization of the deposited films, please refer to the work of Jagosz et al.[22] After 400 cycles, a 34 nm thick poly-crystalline MoS_2 film was deposited. The thickness of the polycrystalline MoS_2 was verified by spectroscopic ellipsometry (SENTECH Instruments GmbH, Model SE800-DUV). The measurement is performed under an angle of 70° and a wavelength range from 190 to 930 nm. By using the software Spectra Ray 4 and the Tauc–Lorentz model for MoS_2, its thickness is calculated.

2.2. Generation of LIPSS

For the generation of the LIPSS in MoS_2 a femtosecond pulsed laser (Light Conversion, Lithuania, model Carbide) was used. The following parameters have been chosen for the experiments: λ = 1030 nm, t_p = 191 fs–10 ps, repetition rate of f_{rep} = 200 kHz–2 MHz, and a natural atmosphere. The laser fluence F was

adjusted with 8 mJ cm^{-2} < F < 130.0 mJ cm^{-2} for all repetition rates by a half - wavelength ($\lambda/2$-wave plate) and a polarization beam splitter. The laser beam is guided to a galvanometer scanner and focused on the sample surface with a F-Θ lens, with a beam waist $\omega_0 \gtrsim 15.0$ µm. The scan speed of the galvanometer scanner was varied between 1 mm s^{-1} $\leqslant v_{scan} \leqslant$ 1000 mm s^{-1}, resulting in pulse per site values of 280 000 $\geqslant O \geqslant$ 28 depending on the laser repetition rate. The galvanometer scanner covered rectangular areas by a set of parallel lines. Each line was shifted vertically by Δy = 5 µm. The laser fluence F was calculated by applying Equation (1), with the pulse energy E_P and the average laser power P_L.

$$F = \frac{E_P}{\pi {\omega_0}^2} \quad \text{with } E_P = \frac{P_L}{f_{rep}} \tag{1}$$

The pulses per site O was calculated by applying Equation (2), with the beam waist diameter $2\omega_0$ and the shift in x - and y - direction (Δx and Δy).

$$O = \frac{\pi {\omega_0}^2}{\Delta x \Delta y} \quad \text{with } \Delta x = \frac{v_{scan}}{f_{rep}} \tag{2}$$

2.3. Characterization

The different LIPSS regions were obtained, using an Olympus LEXT 3D Measuring Laser Microscope OLS5000-SAF with a LM-PlandFL N 50x objective.

Scanning electron microscope (SEM) images were captured with a Schottky field emission microscope Leo Gemini 982 at 2kV.

To assess the microstructure of the film, site-specific cross-sectional transition electron microscope (TEM) lamellas were prepared using a dual-beam FEI Helios G4 CX focused ion beam (FIB) operated at 30 kV. To reduce milling artifacts and damage, the samples were first coated with carbon. In the final thinning step, 8 kV beam was used to minimize the beam damage. Cross section TEM imaging was performed using a JEOL JEM-ARM200F instrument operated at 200 kV.

3. Results

As in our previous publication[21] we varied the laser fluence F and the pulses per site n in every single experiment (see Section 2.2). Furthermore, the repetition rate is varied between 200 kHz $\leqslant f_{rep} \leqslant$ 2 MHz. On behalf of light microscopy images, see Figure S1 (Supporting Information), four main topographic regions could be distinguished. For a better overview in the further, analysis the regions are assigned to colors. **Figure 1** shows the LIPSS regions that form during the processing of the MoS_2 film with f_{rep} = 200 kHz (a) and f_{rep} = 2 MHz (b) with t_p = 200 fs. The pulses per site range goes from O = 720 to O = 72000 pls per site. Both diagrams show, that with fluences F < 20 mJ cm^{-2} only an optical modification (see Figure S1a, Supporting Information, cyan color) of the film is visible independent from the pulses per site, except for the highest pulses per site at f_{rep} = 200 kHz. This modification also appeared in other studies of ours and is associated with a change in crystallinity.[24,25] At higher fluences the formation of LSFL (see Figure S1b, Supporting Information, light-green color) is visible for all pulses per site. These LFSL with the period $\Lambda \approx 0.9\,\mu m$ consist of parallel stripes filled with perpendicularly orientated HSFL (Figure 1d), reproducing our results in the previous study. The formation of the LSFL appears parallel to the polarization of the laser, whereas the HSFL always forms perpendicular to the polarization. However, for a lower number of pulses per site, the MoS_2 film starts to get ablated with simultaneous formation of LSFL (dark-green color). This negative accumulation effect is more dominant for the higher repetition rate f_{rep} = 2 MHz. Upon increasing the fluence, the LSFL formation disappears again and only HSFL covers the whole laser-processed area, see Figure S1c, Supporting Information and Figure 1e. These regions are marked by yellow color and labeled as "HSFL". At even higher fluences the film starts to get ablated (see Figure S1d, Supporting Information, red color). Here again is the negative accumulation effect visible: the ablation is easier for a "lower" number of pulses per site.

TEM images give a more detailed insight into the structure of the LIPSS. **Figure 2**b,c shows TEM images of LSFL and HSFL. Both LIPSS structures are generated by the same parameters (F = 26.2 mJ cm^{-2} and O = 45000 pls per site at f_{rep} = 200 kHz and t_p = 1000 fs) and are extracted transversal (b) blue rectangle) and longitudinal (c) red rectangle) to the LSFL, see in Figure 2a. As one can see in Figure 2c the LSFL pattern is not dominant pronounced, with a closed film on the whole sample. But the sample shows elevations in the period distance, that can also be seen in the SEM images. Interestingly, the accumulated material can be seen on the surface of the MoS_2 film. In contrast to the LSFL the HSFL interrupt the film and form single channels of MoS_2, see Figure 2b. The period of the HSFL is $\Lambda \approx 60 - 70\,nm$ and the height is close to the initial thickness of the film.

For the investigation of the LIPSS formation depending on the pulse duration the latter is varied between 200 fs $\leqslant t_p \leqslant$ 10 ps. **Figure 3** shows the LIPSS formation regions for O = 2800 and O = 28000 pls per site for f_{rep} = 200 kHz, f_{rep} = 400 kHz, f_{rep} = 1 MHz, and f_{rep} = 2 MHz. For f_{rep} = 200 kHz the LSFL forms up to pulse durations t_p = 1000 fs independent on the pulses overlap. For higher O the LFSL starts to form at lower fluences, but the HSFL formation start at the same fluences. Overall are the regions for ablation and HSFL appearance similar for f_{rep} = 200 kHz. The similarity in the region over the pulse overlap can also be found by increased repetition rates (f_{rep} = 400 kHz and f_{rep} = 1 MHz). The main difference to f_{rep} = 200 kHz is, that at O = 2800 pls per site the LSFL form additionally at t_p = 5000 fs. If the repetition rate is increased to f_{rep} = 2 MHz the regions for t_p < 1000 fs are comparable to the regions corresponding to other repetition rates. For longer pulse durations the start and end fluence for LSFL decreases, which implies a lower start frequency for the HSFL formation. The most remarkable difference between pulse durations shorter and longer t_p = 1000 fs is the reduction in the ablation threshold, that decreases for roughly ΔF = 20 mJ cm^{-2}. This could be due to a temperature

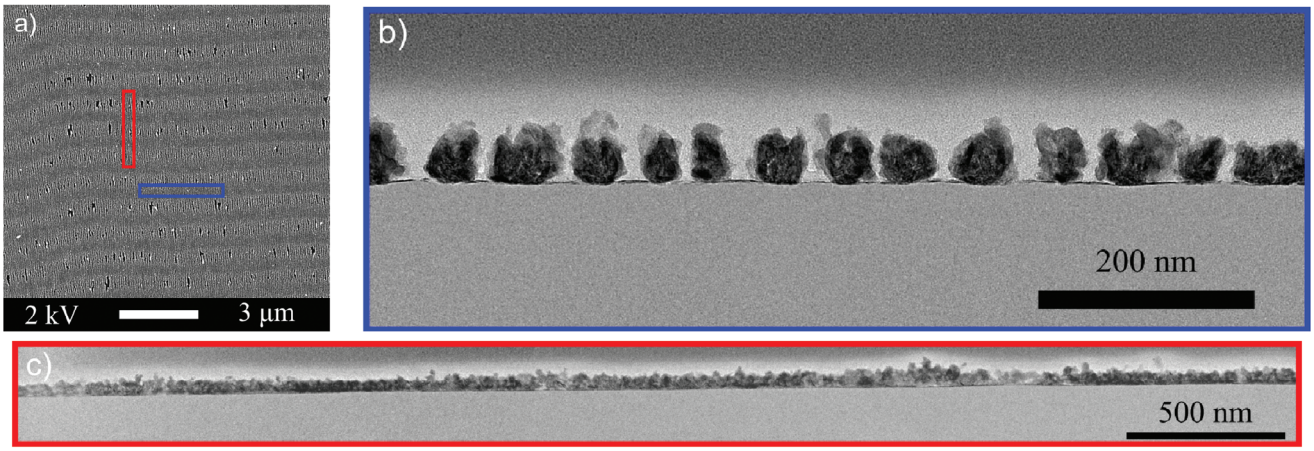

Figure 2. TEM images of the LSFL and HSFL produced with $F = 26.2$ mJ cm^{-2} and $O = 45\,000$ pls per site ($f_{rep} = 200$ kHz and $t_p = 1000$ fs). a) indicates the position and direction of the extracted samples for the TEM measurements. b) TEM image with 50k magnification of the HSFL, which interrupts the film to the surface. c) TEM image with 20k magnification of the LSFL, which form a closed film with slight material accumulation in the period of the LSFL.

accumulation, that only appears due to the combination of the longer pulse durations and the highest repetition rate. The comparison of the plots corresponding to different numbers of pulses per site shows, that at longer pulse durations the film starts to get disrupted/ ablated at fluences $F > 35$ mJ cm^{-2}. This indicates, that the negative accumulation effect also exists at longer pulse durations.

4. Discussion

4.1. Increase in the Pulse Energy

As one can see from the parameter diagrams (see Figures 1a,b and 3), increasing the pulse energy the unperturbed MoS_2 surface is first destabilized to a LSFL structure, consisting of coexisting unperturbed stripes and stripes filled with HSFL. A further increase in the pulse energy increases the fraction of the surface filled with HSFL and the LSFL structure disappears. The ablation starts at even higher pulse energies.

We can explain this sequence of transitions based on the following toy model, which describes this process as an interplay between the wave interference and hydrodynamic-like processes.[7] The interference between the incident and surface-scattered waves results in a periodic temperature profile on the MoS_2 surface as it happens in other materials.[8] However the final step of the model describing how this temperature pattern induces the surface-height profile can have some features specific for the molybdenum disulfide. Along with the possibility that the material rearrangement happens in the liquid MoS_2 due to the development of hydrodynamic instabilities or dewetting in the interference-induced periodic channels,[26] temperature-activated chemical reactions can also induce the nano-patterns.[27] For example, we can speculate that either the decomposition of the MoS_2 to molybdenum and sulfur[28] or oxidation with the formation of gaseous sulfur oxides takes place in the antinodes of the surface temperature distribution. The periodic patterns are known to develop in chemical reactions and the orientation of such patterns is usually perpendicular to the shape of the domain in which the reaction takes place.[29] This explains why the HSFL are oriented perpendicular to the interference stripes forming the LSFL structure. We suppose that the HSFL formation process is activated by the surface temperature and this structure is formed e.g., either due to hydrodynamic flow in the molten material or due to thermal decomposition.[28] Hence there is a threshold for the HSFL formation F_{HSFL} in MoS_2 and we assume that this threshold is below the ablation threshold F_{th}. From a well-accepted hypothesis that the LSFL is formed due to interference between the incident and the surface-scattered wave,[8] we conclude, that at a certain low pulse energy, the temperature profile at the surface[7] overcomes the F_{HSFL} in the maxima of the interference pattern, see **Figure** 4a. The HSFL is formed in stripes on the surface, which period corresponds to the LSFL period and the width of the area where the temperature overcomes the HSFL formation threshold. When the pulse energy (or pulse fluence) increases, but the modulation of the surface temperature is not large, the minimum and the maximum of the surface temperature can be between the thresholds of ablation and FSFL formation, so that the surface is nearly completely covered by HSFL, see Figure 4b. At a higher fluence, the maxima of the temperature overcome the ablation threshold and a periodic ablation pattern overlaps the HSFL structure, see Figure 4c. The period of the ablation pattern again corresponds to LSFL, which can be seen in **Figure** 5b,c more clearly.

4.2. Increase in the Pulse Duration

As it usually happens in laser ablation with ultrafast lasers, the role of thermal effects grows with the laser-pulse duration. If the HSFL structure is formed by hydrodynamic-like processes (which can be "hydrodynamics" in a broad sense, i.e., either a classical flow in thin molten layers, or a chemical reaction,[28] or a nonlinear process activated by the temperature flow at the surface) then the effect of this process should grow with the period of time during which the MoS_2 remains at an elevated

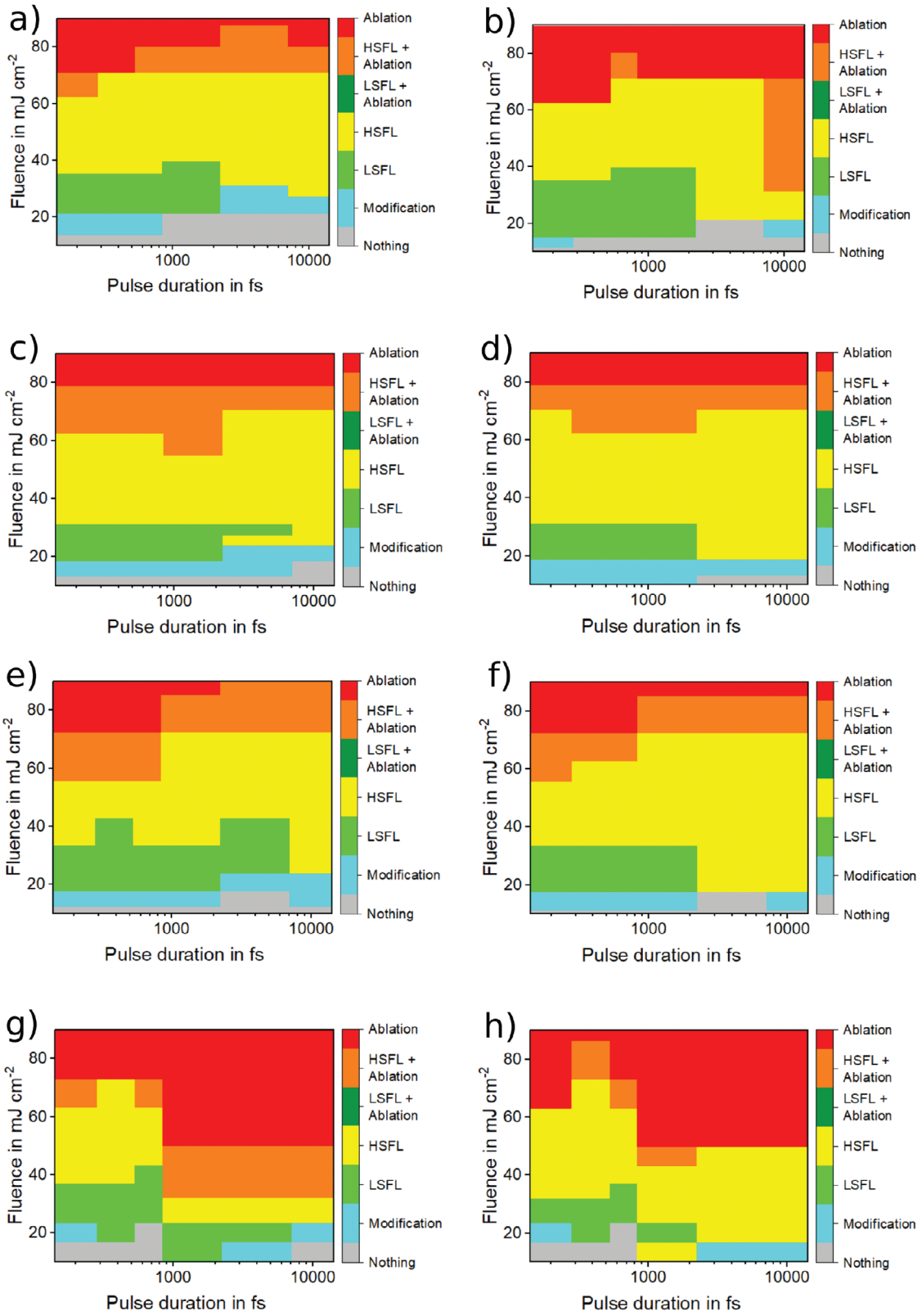

Figure 3. Fluence and pulse duration depended on LIPSS appearance in a 40 nm thick MOS_2 film on SiO_2/Si substrate, a) f_{rep} = 200 kHz with O = 2800 pls per site; b) f_{rep} = 200 kHz with O = 28000 pls per site; c) f_{rep} = 400 kHz with O = 2800 pls per site; d) f_{rep} = 400 kHz with O = 28000 pls per site; e) f_{rep} = 1000 kHz with O = 2800 pls per site; f) f_{rep} = 1000 kHz with O = 28000 pls per site; g) f_{rep} = 2000 kHz with O = 2800 pls per site; h) f_{rep} = 2000 kHz with O = 28000 pls per site.

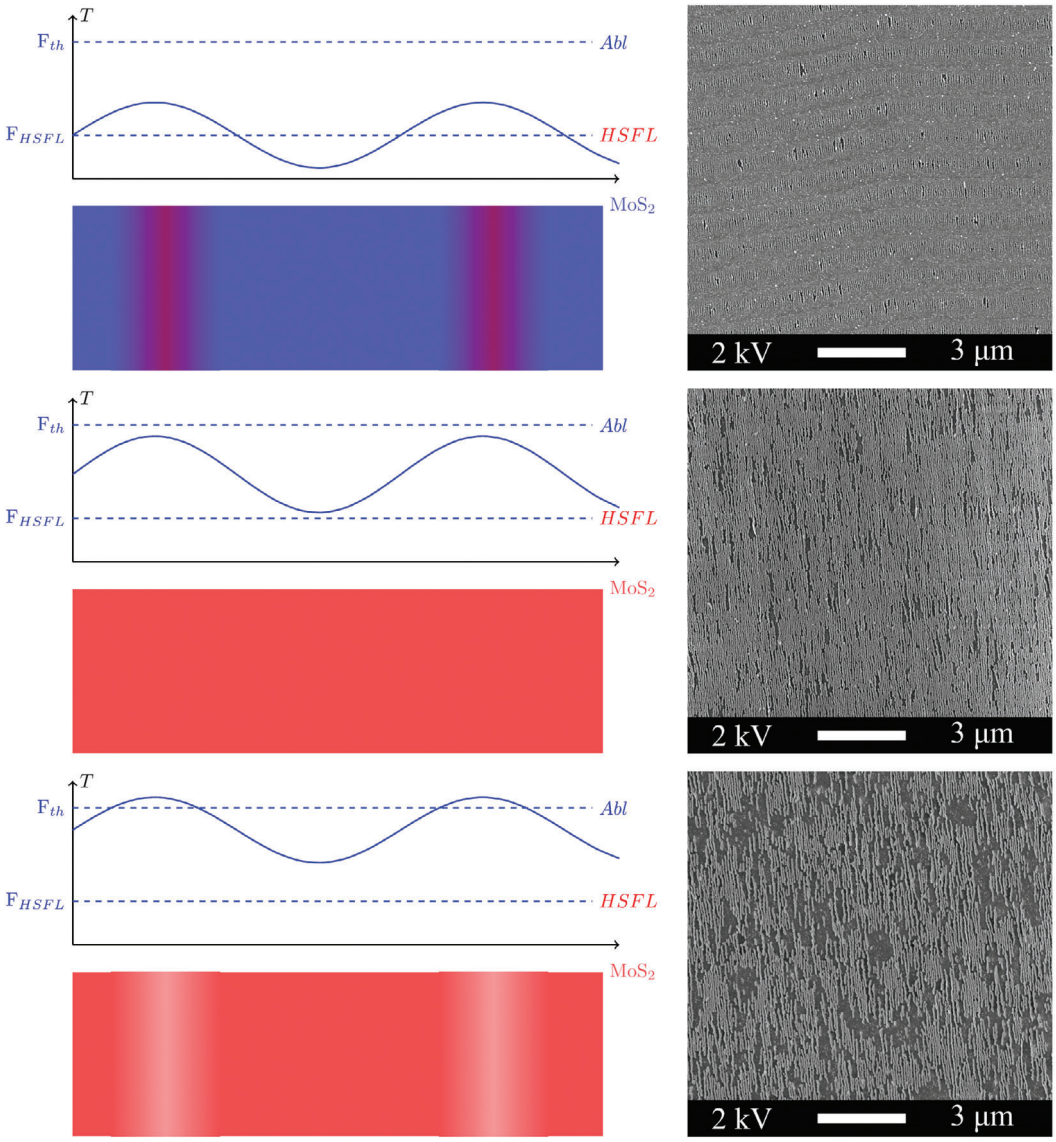

Figure 4. Transition from LSFL to HSFL and to ablation induced by the increasing pulse energy (fluence). The SEM images on the right-hand side correspond to a) $F = 21$ mJ cm^{-2}, $O = 230000$ pls per site and $t_p = 400$ fs; b) $F = 44$ mJ cm^{-2}, $O = 230000$ pls per site and $t_p = 400$ fs and c)$F = 78.5$ mJ cm^{-2}, $O = 46\,000$ pls per site and $t_p = 200$ fs.

temperature. The latter is usually longer for longer laser pulses,[30] Thus, the transition from the combined LSFL/HSFL structure to pure HSFL for longer pulse durations supports the assumption, that the high-spatial frequency LIPSS appear as a pure hydrodynamic self-organisation process.

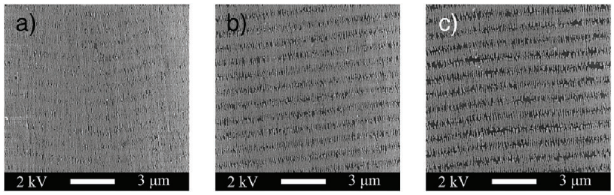

Figure 5. SEM images of LIPSS on the MoS_2 surface processed with $F = 40$ mJ cm^{-2}, $t_p = 1000$ fs, $f_{rep} = 200$ kHz and different scanning speeds v (pulse overlaps O): a) $v = 0.5$ mm s^{-1}, $O = 46000$ pls per site; b) $v = 5$ mm s^{-1}, $O = 4600$ pls per site; c) $v = 20$ mm s^{-1}, $O = 1200$ pls per site.

4.3. Increase in the Pulse Overlap

A set of surface morphologies observed on the MoS_2 surface is shown in Figure 5. One can see that the fraction of the surface, at which the MoS_2 layer was completely removed, grows with the velocity, i.e., by increasing the number of pulses per site at a fixed pulse energy we reduce the ablation, so that more material remains on the substrate. This observation contradicts the results reported for transparent materials,[31,32] in which an increase in the number of pulses per site reduces the ablation threshold.

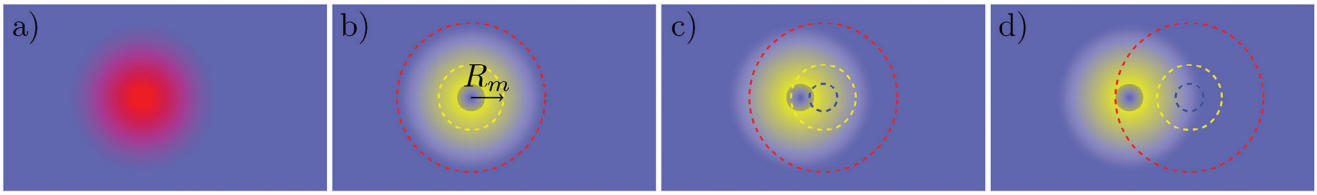

Figure 6. Schematic explanation of the negative incubation model based on the assumption of a modified MoS_2 layer: a) Gaussian profile of the first incident laser pulse with the amplitude slightly exceeding the MoS_2 ablation threshold, the intensity of the red color is proportional to the temperature; b) small ablated spot in the middle is surrounded by a modified area with a higher ablation threshold of a radius R_m; c) if $\Delta x < R_m$, then the next pulse interacts with the modified surface and does not ablate it due to the increased ablation threshold; d) if the distance between the pulses $\Delta x > R_m$, the second pulse also ablates the surface. The temperature field generated by each next pulse extends the modified area so that the following pulses cause no ablation.

Two possible mechanisms of this negative incubation effect can be suggested.

1) There is a threshold for MoS_2 modification, which is below the ablation threshold. The exact nature of this modification is not clear, this can be for example either recrystallization or annealing, or an increase in the surface reflecticity; this question is out of the scope of this paper. We suppose that this modification either increases the ablation threshold of the material or decreases the absorbed laser energy, i.e., makes the ablation more difficult. Let us consider the ablation process starting from the first laser pulse in two cases: i) the pulse overlap is large, i.e., the shift of the laser spot over the sample surface is smaller than the radius of the modification R_m, see **Figure** 6b. If $\Delta x < R_m$, then the next pulse interacts with the modified surface and does not ablate it due to the increased ablation threshold, see Figure 6c. ii) If the pulse overlap is large, i.e., $\Delta x > R_m$, the next pulse reaches a not-modified area with a low ablation threshold and also ablates the surface, see Figure 6d. The fraction of the ablated surface is large in this case.
2) The other model is based on the assumption that the ablation mechanism is the photo-mechanical stress due to thermal extension and the temperature decay time is comparable with the time delay between two pulses. Let us consider the temporal profile of the surface temperature measured in a certain distance from the center of the first pulse, which is comparable with the thermal diffusion length ℓ_{th}. The first near-threshold pulse ablates the surface with a certain probability less than 100%. The temperature at the chosen point increases slightly with a certain delay needed for the heat from the first pulse to reach it and starts decaying afterward. The second pulse comes closer to the chosen point, the temperature there starts growing from an elevated value and decays slower, because the temperature difference between it and the "cold" surrounding is smaller. If the $\Delta x \ll \ell_{th}$, the temperature at the center of each laser spot rises abruptly without preheating causing strong thermal stress and a higher probability of ablation.

However, a simple estimation shows, that the diffusion length estimated with the thermal diffusivity $D_T = 4 \times 10^{-5}\,m^2s^{-1}$ in all experiments is about $\ell_{th} \approx 10\,\mu m$ i.e., is comparable with the laser spot diameter. The laser spot shifts from pulse to pules on $5 \times 10^{-4}\,\mu m < \Delta x < 5\,\mu m$, i.e., $2\omega_0 + \ell_{th} \gg \Delta x$, which makes the first suggested explanation more probable.

5. Conclusion

In this paper, we study the influence of the pulse duration and the repetition rate on the formation of LSFL and HSFL in ALD MoS_2. Due to the disappearance of the LFSL at longer pulses, we concluded that the HSFL formation is due to the hydrodynamic self-organization process. Furthermore, we proposed, that the formation of LSFL is due to the interference of the incident and surface-scattered waves, which leads to fluence maxima, in which the HSFL are formed due to some self-organization process. In addition, chemical modification of the layer can play an important role in the LIPSS formation in MoS_2. For example, oxidation is known to be responsible for positive feedback needed for the LIPSS formation in thin metal films.[9,11] Here similar chemical reactions can provide additional feedback mechanisms due to localized changes in the reflectivity or thermal constants due to phase changes or chemical decomposition of the layer. This decomposition can also explain the negative accumulation effect due to the higher reflectivity of metallic molybdenum, which content on the surface should increase pulse to pulse. Several attempts to measure the chemical composition of the LIPSS structure on the sub-micrometer scale have been undertaken recently by different groups,[33] but the spatial resolution of the available methods does not enable to prove or disprove this assumption. In order for this novel laser-based technology to be used for real devices such as nano-wire transistors in the future, further studies are required, such as investigation of LIPSS formation in film stacks or the formation of LSFL and HSFL in thinner films/ monolayer.

Supporting Information

Supporting Information is available from the Wiley Online Library or from the author.

Acknowledgements

The authors are grateful for financial support from the Federal Ministry of Education and Research of Germany (BMBF) within the ForMikro project FlexTMDSense (grant number 16ES1096K) and the ForLab PICT2DES (grant number 16ES0941) and the Deutsche Forschungsgemeinschaft (DFG-SPP 1796) within FFlexCom (grant number BO2495-3-1).

Open Access funding enabled and organized by Projekt DEAL.

Conflict of Interest

The authors declare no conflict of interest.

Data Availability Statement

The data that support the findings of this study are available from the corresponding author upon reasonable request.

Keywords

2-D materials, femtosecond laser, LIPSS, molybdenum disulfide, periodic structures

Received: May 30, 2024
Revised: September 3, 2024
Published online:

[1] M. Birnbaum, *J. Appl. Phys.* **1965**, *36*, 3688.
[2] J. Bonse, J. Krüger, S. Höhm, A. Rosenfeld, *J. Laser Appl.* **2012**, *24*, 4.
[3] S. Maragkaki, T. J.-Y. Derrien, Y. Levy, N. M. Bulgakova, A. Ostendorf, E. L. Gurevich, *Appl. Surf. Sci.* **2017**, *417*, 88.
[4] S. Maragkaki, A. Elkalash, E. L. Gurevich, *Appl. Phys. A* **2017**, *123*, 1.
[5] W. Gao, K. Zheng, Y. Liao, H. Du, C. Liu, C. Ye, K. Liu, S. Xie, C. Chen, J. Chen, Y. Peng, Y. Leng, *Adv. Mater. Interfaces* **2023**, *10*, 2201924.
[6] J. Bonse, S. Gräf, *Laser Photonics Rev.* **2020**, *14*, 2000215.
[7] E. L. Gurevich, Y. Levy, N. M. Bulgakova, *Nanomaterials* **2020**, *10*, 1836.
[8] D. C. Emmony, R. P. Howson, L. J. Willis, *Appl. Phys. Lett.* **1973**, *23*, 598.
[9] B. Öktem, I. Pavlov, S. Ilday, H. Kalaycıoğlu, A. Rybak, S. Yavaş, M. Erdoğan, F. Ö. Ilday, *Nat. Photonics* **2013**, *7*, 897.
[10] A. V. Dostovalov, V. P. Korolkov, V. S. Terentyev, K. A. Okotrub, F. N. Dultsev, S. A. Babin, *Quantum Electron.* **2017**, *47*, 631.
[11] A. V. Dostovalov, T. J.-Y. Derrien, S. A. Lizunov, F. Přeučil, K. A. Okotrub, T. Mocek, V. P. Korolkov, S. A. Babin, N. M. Bulgakova, *Appl. Surf. Sci.* **2019**, *491*, 650.
[12] K. Bronnikov, A. Dostovalov, V. Terentyev, S. Babin, A. Kozlov, E. Pustovalov, E. L. Gurevich, A. Zhizhchenko, A. Kuchmizhak, *Appl. Phys. Lett.* **2021**, *119*, 211106.
[13] E. Sutter, P. Sutter, *ACS Appl. Nano Mater.* **2018**, *1*, 1042.
[14] H. Y. Lee, S. Kim, *Nanophotonics* **2022**, *11*, 2571.
[15] S. Zhang, R. Li, Z. Yao, P. Liao, Y. Li, H. Tian, J. Wang, P. Liu, J. Guo, K. Liu, F. Mei, L. Liu, *Nanotechnology* **2020**, *31*, 30LT02.
[16] S. W. Kim, J. H. Na, W. L. Choi, H.-J. Chung, S. H. Jhang, S. H. Choi, W. Yang, S. W. Lee, *J. Korean Phys. Soc.* **2016**, *69*, 1505.
[17] A. Beltaos, A. G. Kovačević, A. Matković, U. Ralević, S. Savić-Šević, D. Jovanović, B. M. Jelenković, R. Gajić, **2014**, *116*, 204306.
[18] M. Kasischke, S. Maragkaki, S. Volz, A. Ostendorf, *Evgeny L. Gurevich* **2018**, *445*, 197.
[19] P. Zuo, L. Jiang, X. Li, M. Tian, C. Xu, Y. Yuan, P. Ran, B. Li, Y. Lu, *ACS Appl. Mater. Interfaces* **2019**, *11*, 39334.
[20] I. A. Salimon, E. V. Zharkova, A. V. Averchenko, J. Kumar, P. Somov, O. A. Abbas, P. G. Lagoudakis, S. Mailis, *Micromachines* **2023**, *14*, 1036.
[21] M. J. M. J. Becher, J. Jagosz, C. Bock, A. Ostendorf, E. L. Gurevich, *Front. Nanotechnol.* **2023**, *5*, 1227025.
[22] J. Jagosz, L. Willeke, N. Gerke, M. J. M. J. Becher, P. Plate, A. Kostka, D. Rogalla, A. Ostendorf, C. Bock, *Adv. Mater. Technol.* **2024**, 2400492.
[23] A. Sharma, M. A. Verheijen, L. Wu, S. Karwal, V. Vandalon, H. C. M. Knoops, R. S. Sundaram, J. P. Hofmann, W. M. M. Kessels, A. A. Bol, *Nanoscale* **2018**, *10*, 8615.
[24] M. J. M. J. Becher, J. Jagosz, R.-M. Neubieser, J.-L. Wree, A. Devi, M. Michel, C. Bock, E. L. Gurevich, A. Ostendorf, *Adv. Eng. Mater.* **2023**, *25*, 21.
[25] M. J. M. J. Becher, L. Willeke, C. Bock, A. Ostendorf, in *Laser + Photonics for Advanced Manufacturing*, (Eds.: F. Courvoisier, S. Lecler, W. Pfleging), Proceedings of SPIE. SPIE, Bellingham, Washington, USA **2024**, 40.
[26] K. Khare, M. Brinkmann, B. M. Law, E. L. Gurevich, S. Herminghaus, R. Seemann, *Langmuir* **2007**, *23*, 12138.
[27] A. A. Manshina, I. I. Tumkin, E. M. Khairullina, M. Mizoshiri, A. Ostendorf, S. A. Kulinich, S. Makarov, A. A. Kuchmizhak, E. L. Gurevich, *Adv. Funct. Mater.* **2024**, 2405457.
[28] C. Pan, L. Jiang, J. Sun, Q. Wang, F. Wang, K. Wang, Y. Lu, Y. Wang, L. Qu, T. Cui, *Light Sci. Appl.* **2020**, *9*, 80.
[29] J. D. Murray, *Mathematical Biology: I. An Introduction*, 3rd ed., Springer, New York **2002**.
[30] S. Küper, M. Stuke, *Microelectron. Eng.* **1989**, *9*, 475.
[31] M. Lenzner, J. Krüger, W. Kautek, F. Krausz, *Appl. Phys. A* **1999**, *69*, 465.
[32] S. Xiao, B. Schöps, A. Ostendorf, *Phys. Procedia* **2012**, *39*, 594.
[33] K. Müller, F. Mirabella, X. Knigge, M. Mezera, M. Weise, M. Sahre, K. Wasmuth, H. Voss, A. Hertwig, J. Krüger, J. Radnik, V.-D. Hodoroaba, J. Bonse, *Phys. Status Solidi A* **2024**, *221*, 15.